Super-resolution image reconstruction

Low-resolution Frame

Super-resolution image reconstruction

High-resolution Frame

Chan, Chan, Shen and Shen, Wavelet algorithms for high-resolution image reconstruction, SIAM Journal on Scientific Computing, 24(4), (2003), 1408-1432.

Chan, Riemenschneider, Shen and Shen, Tight Frame: An efficient way for high-resolution image reconstruction, Applied and Computational Harmonic Analysis, 17(1), (2004), 91-115.

Super-resolution image reconstruction from video

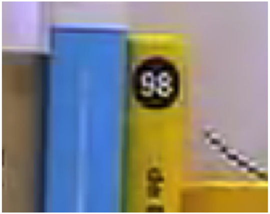

Chan, Shen, Xia, A framelet algorithm for enchancing video stills, Applied and Computational Harmonic Analysis, 23(2) (2007), 153-170.

Convergence

$$\begin{cases} \boldsymbol{c}^* = \arg\min_{\boldsymbol{c}} \{ \frac{1}{2} \| \mathcal{A}\mathcal{W}^T \boldsymbol{c} - \boldsymbol{g} \|_2^2 + \frac{\beta}{2} \| (\mathcal{I} - \mathcal{W}\mathcal{W}^T) \boldsymbol{c} \|_2^2 + \| \mathrm{diag}(\boldsymbol{\lambda}) \boldsymbol{c} \|_1 \}, \\ \boldsymbol{f}^* = \mathcal{W}^T \boldsymbol{c}. \end{cases}$$

Convergence

$$\begin{cases} \boldsymbol{c}^* = \arg\min_{\boldsymbol{c}} \{ \frac{1}{2} \| \mathcal{A}\mathcal{W}^T \boldsymbol{c} - \boldsymbol{g} \|_2^2 + \frac{\beta}{2} \| (\mathcal{I} - \mathcal{W}\mathcal{W}^T) \boldsymbol{c} \|_2^2 + \| \mathrm{diag}(\boldsymbol{\lambda}) \boldsymbol{c} \|_1 \}, \\ \boldsymbol{f}^* = \mathcal{W}^T \boldsymbol{c}. \end{cases}$$

- Sparsity: $\beta = 0$
  - Synthesis-based approach

Convergence

$$\begin{cases} \boldsymbol{c}^* = \arg\min_{\boldsymbol{c}} \{ \frac{1}{2} \| \mathcal{A}\mathcal{W}^T \boldsymbol{c} - \boldsymbol{g} \|_2^2 + \frac{\beta}{2} \| (\mathcal{I} - \mathcal{W}\mathcal{W}^T) \boldsymbol{c} \|_2^2 + \| \mathrm{diag}(\boldsymbol{\lambda}) \boldsymbol{c} \|_1 \}, \\ \boldsymbol{f}^* = \mathcal{W}^T \boldsymbol{c}. \end{cases}$$

- Sparsity: $\beta = 0$
  - Synthesis-based approach
- Sparsity $+$ Regularity: $0 < \beta < +\infty$
  - Balanced approach

Convergence

$$\begin{cases} \boldsymbol{c}^* = \arg\min_{\boldsymbol{c}} \{ \frac{1}{2} \|\mathcal{A}\mathcal{W}^T \boldsymbol{c} - \boldsymbol{g}\|_2^2 + \frac{\beta}{2} \|(\mathcal{I} - \mathcal{W}\mathcal{W}^T)\boldsymbol{c}\|_2^2 + \|\mathrm{diag}(\boldsymbol{\lambda})\boldsymbol{c}\|_1 \}, \\ \boldsymbol{f}^* = \mathcal{W}^T \boldsymbol{c}. \end{cases}$$

- Sparsity: $\beta = 0$
  - Synthesis-based approach
- Sparsity + Regularity: $0 < \beta < +\infty$
  - Balanced approach
- Regularity: $\beta = +\infty$
  - Analysis-based approach

Convergence

$$\begin{cases} \boldsymbol{c}^* = \arg\min_{\boldsymbol{c}} \{ \frac{1}{2} \| \mathcal{A}\mathcal{W}^T \boldsymbol{c} - \boldsymbol{g} \|_2^2 + \frac{\beta}{2} \| (\mathcal{I} - \mathcal{W}\mathcal{W}^T) \boldsymbol{c} \|_2^2 + \| \mathrm{diag}(\boldsymbol{\lambda}) \boldsymbol{c} \|_1 \}, \\ \boldsymbol{f}^* = \mathcal{W}^T \boldsymbol{c}. \end{cases}$$

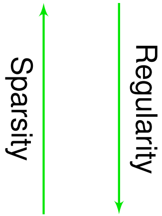

- Sparsity: $\beta = 0$
  - Synthesis-based approach
- Sparsity + Regularity: $0 < \beta < +\infty$
  - Balanced approach
- Regularity: $\beta = +\infty$
  - Analysis-based approach

Convergence

$$\begin{cases} \boldsymbol{c}^* = \arg\min_{\boldsymbol{c}} \{ \frac{1}{2} \| \mathcal{A}\mathcal{W}^T \boldsymbol{c} - \boldsymbol{g} \|_2^2 + \frac{\beta}{2} \| (\mathcal{I} - \mathcal{W}\mathcal{W}^T) \boldsymbol{c} \|_2^2 + \| \mathrm{diag}(\boldsymbol{\lambda}) \boldsymbol{c} \|_1 \}, \\ \boldsymbol{f}^* = \mathcal{W}^T \boldsymbol{c}. \end{cases}$$

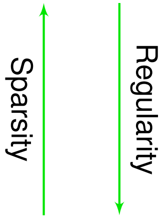

- Sparsity: $\beta = 0$
  - Synthesis-based approach
- Sparsity + Regularity: $0 < \beta < +\infty$
  - Balanced approach
- Regularity: $\beta = +\infty$
  - Analysis-based approach

ℓ_0 minimization model: applying hard-threshold instead

Bao, Dong, Hou, Shen and Zhang, Extrapolated Proximal Iterative Hard Thresholding Methods For Wavelet Frame Based Image Restoration

Iterative algorithms with threshold at each step

Chan, Chan, Shen and Shen, Wavelet algorithms for high-resolution image reconstruction, SIAM Journal on Scientific Computing, 24(4), (2003), 1408-1432.

Chan, Riemenschneider, Shen and Shen, Tight Frame: An efficient way for high-resolution image reconstruction, Applied and Computational Harmonic Analysis, 17(1), (2004), 91-115.

Chai and Shen, Deconvolution: A wavelet frame approach, Numerische Mathematik, 106(4), (2007), 529-587.

Cai, Chan and Shen, A framelet-based image inpainting algorithm, Applied and Computational Harmonic Analysis, 24(2), (2008), 131-149.

Cai, Chan, Shen and Shen, Restoration of chopped and nodded images by framelets, SIAM Journal on Scientific Computing, 30(3), (2008), 1205-1227.

Cai, Chan, Shen and Shen, Simultaneously inpainting in image and transformed domains, Numerische Mathematik, 112(4), (2009), 509-533.

Cai and Shen, Framelet based deconvolution, Journal of Computational Mathematics , 28(3), (2010), 289-308.

Goldstein and Osher, The split Bregman method for L_1-regularized problems, SIAM Journal on Imaging Sciences, 2(2), (2009), 323-343.

Shen, Toh and Yun, An accelerated proximal gradient algorithm for frame-based image restoration via the balanced approach, SIAM Journal on Imaging Sciences, 4(2), (2011), 573-596.

This works for the low rank matrix completion

- Problem: For given $P_\Omega X$ as known entries of a low rank matrix X, how to recover the rest missing entires of X.

This works for the low rank matrix completion

- Problem: For given $P_\Omega X$ as known entries of a low rank matrix X, how to recover the rest missing entires of X.
- Most of such matrices can be recovered by solving:

$$\min_M \{\|M\|_* : P_\Omega M = P_\Omega X\}.$$

Candes and Recht, Exact matrix completion via convex optimization, Found. Comput. Math., 9 (2009), 717-772 .

This works for the low rank matrix completion

- Problem: For given $P_\Omega X$ as known entries of a low rank matrix X, how to recover the rest missing entires of X.
- Most of such matrices can be recovered by solving:

$$\min_M \{\|M\|_* : P_\Omega M = P_\Omega X\}.$$

Candes and Recht, Exact matrix completion via convex optimization, Found. Comput. Math., 9 (2009), 717-772 .

- Low rank

This works for the low rank matrix completion

- Problem: For given $P_\Omega X$ as known entries of a low rank matrix X, how to recover the rest missing entires of X.
- Most of such matrices can be recovered by solving:

$$\min_M \{\|M\|_* : P_\Omega M = P_\Omega X\}.$$

Candes and Recht, Exact matrix completion via convex optimization, Found. Comput. Math., 9 (2009), 717-772 .

- Low rank $\Longrightarrow$ sparsity in singular value domain

This works for the low rank matrix completion

- Problem: For given $P_\Omega X$ as known entries of a low rank matrix X, how to recover the rest missing entires of X.
- Most of such matrices can be recovered by solving:

$$\min_{M}\{\|M\|_* : P_\Omega M = P_\Omega X\}.$$

Candes and Recht, Exact matrix completion via convex optimization, Found. Comput. Math., 9 (2009), 717-772 .

- Low rank $\implies$ sparsity in singular value domain $\implies$ thresholding in singular value domain

This works for the low rank matrix completion

- Problem: For given $P_\Omega X$ as known entries of a low rank matrix X, how to recover the rest missing entires of X.
- Most of such matrices can be recovered by solving:

$$\min_M \{\|M\|_* : P_\Omega M = P_\Omega X\}.$$

Candes and Recht, Exact matrix completion via convex optimization, Found. Comput. Math., 9 (2009), 717-772 .

- Low rank $\implies$ sparsity in singular value domain $\implies$ thresholding in singular value domain $\implies$
- **Singular Value Thresholding Algorithm:**

$$\begin{cases} X^k = D_\lambda(Y^k); \\ Y^k = Y^{k-1} + \delta(P_\Omega X - X^k). \end{cases}$$

This works for the low rank matrix completion

- Problem: For given $P_\Omega X$ as known entries of a low rank matrix X, how to recover the rest missing entires of X.
- Most of such matrices can be recovered by solving:

$$\min_M \{\|M\|_* : P_\Omega M = P_\Omega X\}.$$

Candes and Recht, Exact matrix completion via convex optimization, Found. Comput. Math., 9 (2009), 717-772 .

- Low rank $\Longrightarrow$ sparsity in singular value domain $\Longrightarrow$ thresholding in singular value domain $\Longrightarrow$
- **Singular Value Thresholding Algorithm:**

$$\begin{cases} X^k = D_\lambda(Y^k); \\ Y^k = Y^{k-1} + \delta(P_\Omega X - X^k). \end{cases}$$

- It converges.

Cai, Candès and Shen, A singular value thresholding algorithm for matrix completion, SIAM Journal on Optimization, 20(4), (2010), 1956-1982.

Application: video denoising and inpainting

Gaussian noise: $\sigma = 30$; Poisson noise: $\kappa = 15$; SP impulse noise: 20%.

Ji, Liu, Shen and Xu, Robust video denoising using low rank matrix completion, CVPR, 2010.

Ji, Huang, Shen and Xu, Robust video restoration by joint sparse and low rank matrix approximation, SIAM Journal on Imaging Sciences, 4(4), (2011), 1122-1142.

Image restoration: Data-driven tight frame model

- Data-driven balanced approach

$$\min_{\boldsymbol{c},\mathcal{W}} \|\mathcal{A}\mathcal{W}^T\boldsymbol{c} - \boldsymbol{g}\|_2^2 + \frac{\beta}{2}\|(\mathcal{I} - \mathcal{W}\mathcal{W}^T)\boldsymbol{c}\|_2^2 + \|\mathrm{diag}(\boldsymbol{\lambda})\boldsymbol{c}\|_1$$

where $\mathcal{W}$ is the tight frame generated by a set of filters that is adapted to the input data.

Image restoration: Data-driven tight frame model

- Data-driven balanced approach

$$\min_{\boldsymbol{c},\mathcal{W}} \|\mathcal{A}\mathcal{W}^T\boldsymbol{c}-\boldsymbol{g}\|_2^2+\frac{\beta}{2}\|(\mathcal{I}-\mathcal{W}\mathcal{W}^T)\boldsymbol{c}\|_2^2+\|\mathrm{diag}(\boldsymbol{\lambda})\boldsymbol{c}\|_1$$

  where $\mathcal{W}$ is the tight frame generated by a set of filters that is adapted to the input data.

- For denoising, we can have the following ℓ_0 model

$$\min_{\boldsymbol{c},\mathcal{W}} \|\mathcal{W}^T\boldsymbol{c}-\boldsymbol{g}\|_2^2+\|(\mathcal{I}-\mathcal{W}\mathcal{W}^T)\boldsymbol{c}\|_2^2+\lambda^2\|\boldsymbol{c}\|_0$$
$$\text{subject to } \mathcal{W}^T\mathcal{W}=\mathcal{I}.$$

  This problem can be solved by alternating direction method. Both minimizations have analytical solutions. The algorithm converges.

Image restoration: Data-driven tight frame model

- Data-driven balanced approach

$$\min_{\boldsymbol{c},\mathcal{W}} \|\mathcal{A}\mathcal{W}^T\boldsymbol{c} - \boldsymbol{g}\|_2^2 + \frac{\beta}{2}\|(\mathcal{I} - \mathcal{W}\mathcal{W}^T)\boldsymbol{c}\|_2^2 + \|\mathrm{diag}(\boldsymbol{\lambda})\boldsymbol{c}\|_1$$

  where $\mathcal{W}$ is the tight frame generated by a set of filters that is adapted to the input data.

- For denoising, we can have the following ℓ_0 model

$$\min_{\boldsymbol{c},\mathcal{W}} \|\mathcal{W}^T\boldsymbol{c} - \boldsymbol{g}\|_2^2 + \|(\mathcal{I} - \mathcal{W}\mathcal{W}^T)\boldsymbol{c}\|_2^2 + \lambda^2\|\boldsymbol{c}\|_0$$
$$\text{subject to } \mathcal{W}^T\mathcal{W} = \mathcal{I}.$$

  This problem can be solved by alternating direction method. Both minimizations have analytical solutions. The algorithm converges.

Cai, Ji, Shen and Ye, Data-driven tight frame construction and image denoising, Applied and Computational Harmonic Analysis, 37(1), (2014), 89-105.

Bao, Ji, Quan and Shen, L_0 norm based dictionary learning by proximal methods with global convergence, CVPR, 2014.

Bao, Ji and Shen, Convergence analysis for iterative data-driven tight frame construction scheme, Applied and Computational Harmonic Analysis, 2014.

Data-driven tight frame image denoising

image	σ	thresholding	K-SVD		Data-driven tight frame	
			8×8	16×16	8×8	16×16
Barbara	5	36.48	38.14	37.91	38.07	**38.26**
	10	32.10	34.43	33.96	34.26	**34.68**
	15	29.61	32.42	31.73	32.03	**32.51**
	20	27.98	30.93	30.16	30.42	**31.01**
	25	26.73	29.76	28.83	29.27	**29.85**
Cameraman	5	37.49	**37.93**	36.93	37.86	37.81
	10	32.97	**33.71**	32.79	33.59	33.54
	15	30.53	**31.46**	30.42	31.27	31.13
	20	28.89	**29.91**	28.92	29.59	29.61
	25	27.61	**28.91**	27.70	28.51	28.49
Boat	5	36.32	**37.16**	36.63	37.04	37.08
	10	32.81	33.63	32.96	33.65	**33.73**
	15	30.80	31.70	30.81	31.70	**31.77**
	20	29.34	30.31	29.27	30.32	**30.40**
	25	28.23	29.25	28.16	29.21	**29.34**
Couple	5	36.79	37.24	36.78	**37.31**	37.28
	10	33.08	33.50	32.74	33.63	**33.67**
	15	30.94	31.47	30.49	31.54	**31.63**
	20	29.43	30.02	28.97	30.07	**30.21**
	25	28.27	28.84	27.80	28.99	**29.15**

Data-driven tight frame image denoising

image	σ	thresholding	K-SVD		Data-driven tight frame	
			8×8	16×16	8×8	16×16
Fingerprint	5	35.01	**36.61**	36.06	36.58	36.55
	10	30.52	**32.39**	31.80	32.31	32.26
	15	28.12	**30.07**	29.35	29.91	29.92
	20	26.53	**28.44**	27.58	28.33	28.34
	25	25.35	**27.28**	26.32	27.17	27.17
Hill	5	36.33	36.96	36.51	36.96	**36.97**
	10	32.65	33.34	32.72	33.35	**33.35**
	15	30.74	31.43	30.68	31.51	**31.52**
	20	29.43	30.17	29.27	30.21	**30.25**
	25	28.41	29.19	28.24	29.23	**29.31**
Lena	5	37.63	38.56	38.13	38.61	**38.70**
	10	34.17	35.55	34.94	35.52	**35.71**
	15	32.17	33.72	32.98	33.61	**33.83**
	20	30.66	32.39	31.64	32.19	**32.43**
	25	29.46	31.35	30.45	31.05	**31.38**
Man	5	36.77	37.55	36.82	37.58	**37.57**
	10	32.73	33.60	32.68	33.63	**33.65**
	15	30.54	31.45	30.51	31.46	**31.49**
	20	29.09	**30.13**	29.09	30.09	30.08
	25	27.99	**29.11**	27.92	29.03	29.02

Data-driven non-local frame model: Global information helps local feature recovery

- The analysis-based approach

$$\min_{\boldsymbol{f}} \frac{1}{2}\|\mathcal{A}\boldsymbol{f} - \boldsymbol{g}\|_2^2 + \|\text{diag}(\boldsymbol{\lambda})\mathcal{W}\boldsymbol{f}\|_1,$$

Data-driven non-local frame model: Global information helps local feature recovery

- The analysis-based approach

$$\min_{\boldsymbol{f}} \frac{1}{2}\|\mathcal{A}\boldsymbol{f}-\boldsymbol{g}\|_2^2+\|\mathrm{diag}(\boldsymbol{\lambda})\mathcal{W}\boldsymbol{f}\|_1,$$

- The analysis-based approach with the non-local analysis operator

$$\min_{\boldsymbol{f}} \frac{1}{2}\|\mathcal{A}\boldsymbol{f}-\boldsymbol{g}\|_2^2+\|\mathrm{diag}(\boldsymbol{\lambda})\mathcal{D}(\boldsymbol{f})\boldsymbol{f}\|_1$$

where

$$\mathcal{D}(\boldsymbol{f})=\frac{1}{\sqrt{2}}\begin{pmatrix}\mathcal{I}\\ \mathcal{J}(\boldsymbol{f})\end{pmatrix}\mathcal{W}$$

with $\mathcal{J}(\boldsymbol{f})$ being the nonlocal operator derived from the input data.

Quan, Ji and Shen, Data-driven multi-scale non-local wavelet frame construction and image recovery, Journal of Scientific Computing, 2014

Data-driven non-local frame model

Image	Kernel	Loc. frame	Nonloc. TV	BM3DDEB	Nonloc. frame
peppers256	disk	26.14	25.22	28.08	**29.25**
	motion	25.41	24.20	26.60	**28.26**
	gaussian	25.97	25.65	26.29	**27.66**
	box	25.84	25.45	26.67	**27.78**
goldhill256	disk	26.31	25.43	26.65	**26.69**
	motion	25.78	24.44	25.95	**26.19**
	gaussian	26.33	26.29	26.59	**26.83**
	box	25.40	24.87	25.69	**25.78**
boat256	disk	25.23	24.91	25.71	**25.75**
	motion	24.61	23.88	25.06	**25.24**
	gaussian	25.40	25.58	25.64	**25.81**
	box	24.19	24.20	24.56	**24.62**
camera256	disk	25.43	25.43	26.50	**26.82**
	motion	24.97	24.33	25.82	**26.48**
	gaussian	25.44	25.91	26.02	**26.26**
	box	24.16	24.46	24.85	**25.46**

Table 1: Comparison of the PSNR values (dB) of the results from the four algorithms, with respect to the noise level $\sigma = 5$.

Data-driven non-local frame model

Image	Kernel	Loc. frame	Nonloc. TV	BM3DDEB	Nonloc. frame
house256	disk	30.75	29.50	**32.02**	31.88
	motion	29.78	27.28	30.87	**31.03**
	gaussian	30.72	30.54	31.19	**31.52**
	box	29.48	28.66	30.34	**30.79**
fingerp.512	disk	26.87	24.66	27.45	**27.53**
	motion	23.82	22.16	24.91	**25.46**
	gaussian	27.67	27.21	28.08	**28.19**
	box	22.85	22.69	24.02	**24.28**
Barbara512	disk	24.28	24.30	**25.28**	24.72
	motion	24.10	23.73	**25.01**	24.39
	gaussian	24.27	24.15	**24.43**	24.39
	box	23.69	23.54	**24.01**	23.91
Lena512	disk	31.13	28.95	31.72	**31.82**
	motion	29.77	27.45	30.30	**30.42**
	gaussian	31.53	30.63	32.15	**32.17**
	box	29.17	28.18	29.35	**29.75**

Table 1: Comparison of the PSNR values (dB) of the results from the four algorithms, with respect to the noise level $\sigma = 5$.

The piecewise smooth function model

$\mathbf{\Gamma}$: the domain of singularities.
$\mathbf{\Gamma}^c$: the domain of smooth parts of the image.
Aim: keep the edges sharp and the smooth parts smooth.
Key: to locate $\mathbf{\Gamma}$ from data iteratively.

The piecewise smooth function model

Γ: the domain of singularities.
Γ^c: the domain of smooth parts of the image.
Aim: keep the edges sharp and the smooth parts smooth.
Key: to locate Γ from data iteratively.

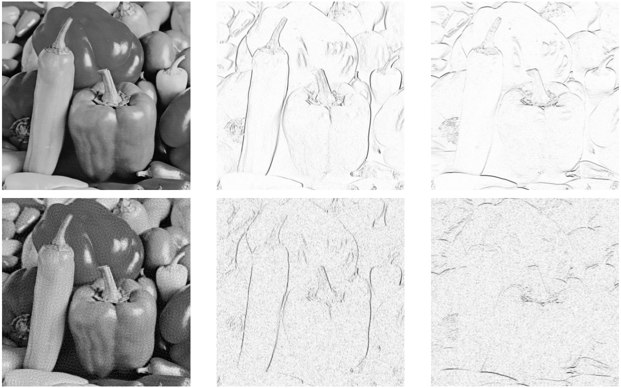

Figure: The first row: the clear image, the supports of its wavelet coefficients with large magnitude in two high-pass channels. The second row: the image recovered by pesudo-inverse filter, the supports of its wavelet coefficients with large magnitude in the same high-pass channels.

Data Driven model for piecewise smooth image

Recall the analysis-based approach

$$\min_{\boldsymbol{f}} \frac{1}{2}\|\mathcal{A}\boldsymbol{f} - \boldsymbol{g}\|_2^2 + \|\mathrm{diag}(\boldsymbol{\lambda})\mathcal{W}_H \boldsymbol{f}\|_1,$$

where

$$\mathcal{W} = \begin{pmatrix} \mathcal{W}_H \\ \mathcal{W}_L \end{pmatrix}.$$

Data Driven model for piecewise smooth image

Recall the analysis-based approach

$$\min_{\boldsymbol{f}} \frac{1}{2}\|\mathcal{A}\boldsymbol{f} - \boldsymbol{g}\|_2^2 + \|\text{diag}(\boldsymbol{\lambda})\mathcal{W}_H \boldsymbol{f}\|_1,$$

where

$$\mathcal{W} = \begin{pmatrix} \mathcal{W}_H \\ \mathcal{W}_L \end{pmatrix}.$$

Data-driven models to identify the position set $\boldsymbol{\Gamma}$ of the features.

$$\min_{\boldsymbol{f},\boldsymbol{\Gamma}} \frac{1}{2}\|\mathcal{A}\boldsymbol{f} - \boldsymbol{g}\|_2^2 + \|\boldsymbol{\gamma} \cdot \mathcal{W}_{\boldsymbol{\Gamma}} \boldsymbol{f}\|_1 + \|\boldsymbol{\lambda} \cdot \mathcal{W}_{\boldsymbol{\Gamma}^c} \boldsymbol{f}\|_2^2$$

Data Driven model for piecewise smooth image

Recall the analysis-based approach

$$\min_{\boldsymbol{f}} \frac{1}{2}\|\mathcal{A}\boldsymbol{f} - \boldsymbol{g}\|_2^2 + \|\mathrm{diag}(\boldsymbol{\lambda})\mathcal{W}_H \boldsymbol{f}\|_1,$$

where

$$\mathcal{W} = \begin{pmatrix} \mathcal{W}_H \\ \mathcal{W}_L \end{pmatrix}.$$

Data-driven models to identify the position set $\boldsymbol{\Gamma}$ of the features.

$$\min_{\boldsymbol{f},\boldsymbol{\Gamma}} \frac{1}{2}\|\mathcal{A}\boldsymbol{f} - \boldsymbol{g}\|_2^2 + \|\boldsymbol{\gamma} \cdot \mathcal{W}_{\boldsymbol{\Gamma}} \boldsymbol{f}\|_1 + \|\boldsymbol{\lambda} \cdot \mathcal{W}_{\boldsymbol{\Gamma}^c} \boldsymbol{f}\|_2^2$$

Cai, Dong and Shen, Image restorations: a wavelet frame based model for piecewise smooth functions and beyond, 2014.

Data driven moedel for piecewise smooth image

Input blurred images

PSNR = 22.5976

PSNR = 24.1189

PSNR = 26.1993

PSNR = 25.9306

Restored images

PSNR = 27.5443

PSNR = 27.8618

PSNR = 30.0355

PSNR = 29.6716

The computed jump set Γ

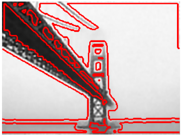

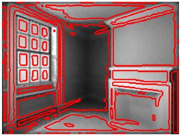

$$\min_{\boldsymbol{f},\boldsymbol{\Gamma}} \frac{1}{2}\|\mathcal{A}\boldsymbol{f} - \boldsymbol{g}\|_2^2 + \lambda^2\|\mathcal{W}_{\boldsymbol{\Gamma}^c}\boldsymbol{f}\|_2^2 : |\boldsymbol{\Gamma}| \le T.$$

Ji, Luo and Shen, Image recovery via geometrically structured approximation, 2015.

Image	Kernel	TV	Framelet	Co-sparsity	Our method
peppers256	disk	24.866	26.3226	25.252	**28.342**
	motion	24.922	26.5812	25.788	**27.243**
	Gaussian	25.078	25.9699	25.081	**27.16**
	average	23.923	26.1198	24.684	**27.17**
goldhill256	disk	25.867	26.4577	26.22	**26.598**
	motion	25.5	26.2752	25.62	**26.265**
	Gaussian	26.056	26.4133	26.303	**26.801**
	average	24.926	25.6087	25.199	**25.718**
boat256	disk	24.638	25.4061	24.846	**25.524**
	motion	24.173	25.0211	24.2	**25.309**
	Gaussian	24.958	25.5148	24.942	**25.589**
	average	23.638	24.4339	23.776	**24.441**
camera256	disk	24.43	25.6798	24.525	**25.879**
	motion	23.653	25.3515	24.737	**25.917**
	Gaussian	24.787	25.5479	24.754	**25.756**
	average	23.17	24.5088	23.678	**24.989**
Barbara512	disk	24.208	24.153	24.2866	**24.34**
	motion	23.571	23.8753	23.573	**23.91**
	Gaussian	24.089	24.2618	24.107	**24.29**
	average	23.45	23.6921	23.486	**23.71**
Lena512	disk	29.939	30.165	31.1621	**31.184**
	motion	27.688	29.3335	28.324	**29.543**
	Gaussian	30.453	31.5336	30.702	**31.7**
	average	28.066	29.17	28.44	**29.21**

Table: Comparison of the PSNR values (dB) of the results by four methods, with respect to the noise level $\sigma = 5$.

Wavelet frame approach and PDE approach

- Cai, Dong, Osher and Shen, Image restoration: total variation, wavelet frames, and beyond, Journal of the American Mathematical Society, 25(4), (2012), 1033-1089.

  In particularly, establish the connection between TV model and tight wavelet frame analysis model.

Wavelet frame approach and PDE approach

- Cai, Dong, Osher and Shen, Image restoration: total variation, wavelet frames, and beyond, Journal of the American Mathematical Society, 25(4), (2012), 1033-1089.

  In particularly, establish the connection between TV model and tight wavelet frame analysis model.

- Dong, Jiang and Shen, Image restoration: wavelet frame shrinkage, nonlinear evolution PDEs, and beyond, 2013.

  Understand the nonlinear solution PDEs in term of wavelet tight frame approach.

Wavelet frame approach and PDE approach

- Cai, Dong, Osher and Shen, Image restoration: total variation, wavelet frames, and beyond, Journal of the American Mathematical Society, 25(4), (2012), 1033-1089.

  In particularly, establish the connection between TV model and tight wavelet frame analysis model.

- Dong, Jiang and Shen, Image restoration: wavelet frame shrinkage, nonlinear evolution PDEs, and beyond, 2013.

  Understand the nonlinear solution PDEs in term of wavelet tight frame approach.

- Cai, Dong and Shen, Image restorations: a wavelet frame based model for piecewise smooth functions and beyond, 2014.

  In particular, connect the Mumford-Shah model to the wavelet tight frame approach.

Wavelet frame approach and PDE approach

- Understand each of three major PDE based models as a wavelet based analysis approach with proper choices of shrinkage and parameters.

Wavelet frame approach and PDE approach

- Understand each of three major PDE based models as a wavelet based analysis approach with proper choices of shrinkage and parameters.
- Give space/time-frequency analysis to PDE approaches and give geometric understanding for frame based approaches.

Wavelet frame approach and PDE approach

- Understand each of three major PDE based models as a wavelet based analysis approach with proper choices of shrinkage and parameters.
- Give space/time-frequency analysis to PDE approaches and give geometric understanding for frame based approaches.
- Provide a method to solve PDE based models with asymptotic convergence analysis as a side product.

Wavelet frame approach and PDE approach

- Understand each of three major PDE based models as a wavelet based analysis approach with proper choices of shrinkage and parameters.
- Give space/time-frequency analysis to PDE approaches and give geometric understanding for frame based approaches.
- Provide a method to solve PDE based models with asymptotic convergence analysis as a side product.
- Make wavelet based approaches go beyond image processing, restoration and reconstruction, e.g. surface processing and reconstruction .

Surface reconstruction

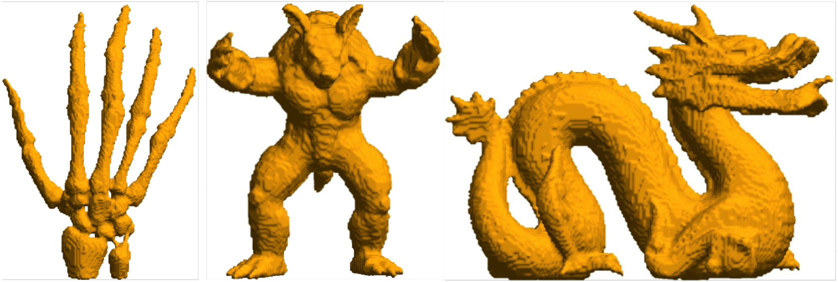

Dong and Shen, Wavelet frame based surface reconstruction from unorganized points, Journal of Computational Physics, 230(22), (2011), 8247-8255.

Dong and Shen, MRA-based wavelet frames and applications: image segmentation and surface reconstruction, SPIE 2012 Defense, Security and Sensing, 8401 Article number: 840102 DOI 10.1117/12.923203, (2012).

Surface denoising: wavelet tight frame on triangle mesh

The botijo4 model | Corrupted by Gaussian noise | Denoised

Dong, Jiang, Liu and Shen, Multiscale representation of surfaces by tight wavelet frames with applications to denoising, 2014.

Wavelet frame approach and PDE approach

Frame based models provide much wider choices. For examples,

- Built-in multi-level structure;

Wavelet frame approach and PDE approach

Frame based models provide much wider choices. For examples,

- Built-in multi-level structure;
- Balanced and synthesis based approaches;

Wavelet frame approach and PDE approach

Frame based models provide much wider choices. For examples,

- Built-in multi-level structure;
- Balanced and synthesis based approaches;
- A wide range of choices of frames, e.g., data-driven frames or Gabor directional frames

Gabor frame as directional frame

A complex-valued tensor product Gabor filter bank:

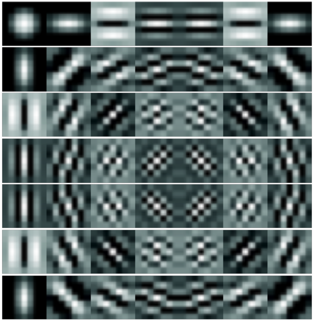

Real Part

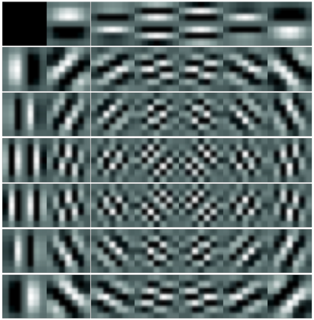

Imaginary Part

Ji, Shen and Zhao, Directional frames for image recovery: multi-scale finite discrete Gabor frames, 2014

Ron and Shen, Frames and stable bases for subspaces of $L_2(\mathbb{R}^d)$: the duality principle of Weyl-Heisenberg sets, Proceedings of the Lanczos Centenary Conference Raleigh, NC, M. Chu, R. Plemmons, D. Brown, and D. Ellison eds., SIAM Pub. (1993), 422-425.

Ron and Shen, Weyl-Heisenberg frames and Riesz bases in $L_2(\mathbb{R}^d)$, Duke Mathematical Journal, 89, (1997), 237-282.

Simulation results for Gabor frame

PSNR value of denoised images:

image	σ	TV	framelet +LDCT	DT CWT	Gabor size:15,7
Barbara512	20	26.84	29.25	28.90	**30.39**
	30	24.82	27.14	26.61	**28.23**
	40	23.87	25.78	24.91	**26.71**
	50	23.22	24.40	23.78	**25.40**
Bowl256	20	29.24	30.15	29.43	**30.58**
	30	27.63	28.51	27.50	**28.84**
	40	26.76	27.42	26.42	**27.81**
	50	26.15	26.68	25.64	**26.80**
Cameraman256	20	28.83	29.00	28.94	**29.26**
	30	26.83	27.18	26.92	**27.43**
	40	25.53	25.73	25.29	**26.00**
	50	24.50	24.55	24.06	**25.03**

Some ideas of proof

PDE approach $E(f) = \frac{1}{2}\int_\Omega (\mathcal{A}f - g)^2 + \nu\|\mathbf{D}f\|_1$.

Some ideas of proof

PDE approach $E(f) = \frac{1}{2}\int_\Omega (\mathcal{A}f - g)^2 + \nu\|\mathbf{D}f\|_1.$

Analysis based approach $E_n(\boldsymbol{f}) = \frac{1}{2}\|\mathcal{A}\boldsymbol{f} - \boldsymbol{g}\|_2^2 + \nu\|\mathrm{diag}(\boldsymbol{\lambda}) \cdot \mathcal{W}_n\boldsymbol{f}\|_1$

Some ideas of proof

PDE approach $E(f) = \frac{1}{2} \int_\Omega (\mathcal{A} f - g)^2 + \nu \|\mathbf{D} f\|_1.$

$E_n(f) = \dots$

↕ Reformulation

Analysis based approach $E_n(\boldsymbol{f}) = \frac{1}{2} \|\mathcal{A} \boldsymbol{f} - \boldsymbol{g}\|_2^2 + \nu \|\mathrm{diag}(\boldsymbol{\lambda}) \cdot \mathcal{W}_n \boldsymbol{f}\|_1$

Some ideas of proof

PDE approach

$$E(f) = \frac{1}{2}\int_\Omega (\mathcal{A}f - g)^2 + \nu \|\mathbf{D}f\|_1.$$

Pointwise ↑

$$E_n(f) = \dots$$

Reformulation ↕

Analysis based approach

$$E_n(\boldsymbol{f}) = \frac{1}{2}\|\mathcal{A}\boldsymbol{f} - \boldsymbol{g}\|_2^2 + \nu\|\mathrm{diag}(\boldsymbol{\lambda}) \cdot \mathcal{W}_n \boldsymbol{f}\|_1$$

Some ideas of proof

PDE approach $E(f) = \frac{1}{2}\int_\Omega (\mathcal{A}f - g)^2 + \nu \|\mathbf{D}f\|_1.$

Pointwise / Gamma-converge

$E_n(f) = \dots$

Reformulation

Analysis based approach $E_n(\boldsymbol{f}) = \frac{1}{2}\|\mathcal{A}\boldsymbol{f} - \boldsymbol{g}\|_2^2 + \nu\|\mathrm{diag}(\boldsymbol{\lambda}) \cdot \mathcal{W}_n \boldsymbol{f}\|_1$

Some ideas of proof

PDE approach $E(f) = \frac{1}{2}\int_\Omega (\mathcal{A}f - g)^2 + \nu \|\mathbf{D}f\|_1.$

Pointwise ↑ ↑ Gamma-converge

$E_n(f) = \ldots$

↕ Reformulation

Analysis based approach $E_n(\boldsymbol{f}) = \frac{1}{2}\|\mathcal{A}\boldsymbol{f} - \boldsymbol{g}\|_2^2 + \nu\|\mathrm{diag}(\boldsymbol{\lambda}) \cdot \mathcal{W}_n \boldsymbol{f}\|_1$

- Let f_n^* be an approximate optimal solution to E_n. Then

$$\limsup_{n\to\infty} E_n(f_n^*) \leq \inf_f E(f),$$

and any cluster point of $\{f_n^*\}$ is an approximate optimal solution to E.

Some ideas of proof

PDE approach: $E(f) = \frac{1}{2}\int_\Omega (\mathcal{A}f - g)^2 + \nu \|\mathbf{D}f\|_1.$

↑ Pointwise ↑ Gamma-converge

$E_n(f) = \ldots$

↕ Reformulation

Analysis based approach: $E_n(\boldsymbol{f}) = \frac{1}{2}\|\mathcal{A}\boldsymbol{f} - \boldsymbol{g}\|_2^2 + \nu\|\mathrm{diag}(\boldsymbol{\lambda}) \cdot \mathcal{W}_n \boldsymbol{f}\|_1$

- Let f_n^* be an approximate optimal solution to E_n. Then

$$\limsup_{n\to\infty} E_n(f_n^*) \le \inf_f E(f),$$

and any cluster point of $\{f_n^*\}$ is an approximate optimal solution to E.

To make this work, use the spline wavelet frame from UEP.

Cai, Dong, Osher and Shen, Image restoration: total variation, wavelet frames, and beyond, Journal of the American Mathematical Society, 25(4), (2012), 1033-1089.

Thank you!

http://www.math.nus.edu.sg/∼matzuows/

Zuowei Shen, Wavelet frames and image restorations, Proceedings of the International Congress of Mathematicians, Vol IV, Hyderabad, India, (2010), Hindustan Book Agency, (Rajendra Bhatia eds), 2834-2863.

Bin Dong and Zuowei Shen, Image restoration: A Data driven perspective, Proceedings of the International Congress on Industrial and Applied Mathematics (2015) .

Bin Dong and Zuowei Shen, MRA-based wavelet frames and applications, IAS/Park City Mathematics Series: The Mathematics of Image Processing, Vol 19, (2010), 7-158.